Refractive index variation rate measurement method based on OAM interferometry and time-frequency analysis

Shuimei Wu, Fenghua Ma, Anting Wang*
Department of Optics and Optical Engineering, University of Science and Technology of China, Hefei 230026, China
*Corresponding author: atwang@ustc.edu.cn

ABSTRACT

A scheme for measuring a small variation rate of the refractive index (RI) based on orbital angular momentum (OAM) interferometry and time-frequency analysis is proposed and demonstrated in this paper. Two vortex beams carrying OAM of opposite signs are used for interference to produce a petal-like intensity distribution. The variation in RI of the sample leads to a time variable phase delay between the reference and measurement paths, and causes the rotation of the petal-like spots. The rotation angular velocity of the petal-like spots is proportional to the RI variation rate, the normalized cross correlation method is used to estimate it. Then, a time-frequency analysis method is employed to study the time evolution of the variation rate of RI. Three kinds of RI models with different variation rates are simulated and the results are consistent with expectations. The proposed measurement method is simple in structure, and extends a new approach to detect other physical coefficients of RI or the tiny velocity.

Keywords: refractive index variation rate, OAM interferometry, time-frequency analysis.

1. INTRODUCTION

Due to the high-sensitivity sensing ability brings from rotational symmetric helical phase structure of the orbital angular momentum (OAM) beam, OAM beams have been widely used in the field of optical sensing measurement[1-6]. The petal-like pattern formed by the interference of two conjugated OAM beams is particularly intriguing to researchers. S. Yu et al. realized a high-precision magnetic field intensity measurement with superposition OAM beams combined with the Faraday effect[7]. J. Zhu et al. proposed a method for detecting the dynamic micro-displacement and direction of a moving object by using a petal-like interference pattern[8]. Z. Zhang et al. obtained a measurement error rate that is less than 10 nm/s by using a system for detecting tiny velocity based on a rotating petal-like light structure and single-point detector[9]. Y. Zhai et al. studied the evolution of angular velocity over time using the interference of OAM beams with opposite helicity[10]. A. H. Dorrah et al. demonstrated a novel refractive index (RI) sensing scheme that can realize the adjustment of the measuring range and measuring precision based on the self-interference of two conjugated OAM modes[11].

Changes in various attributes of the medium, for example density, concentration and temperature will affect the RI of the medium. In addition, the changes in external conditions such as pressure and electromagnetic field intensity will also change the RI of the medium to some extent. In production practice, it is of great significance to measure the variation in the RI of a medium with different properties. The variation rate of RI can reflect its change trend. In this letter, a scheme for measuring the RI variation rate based on the interference of OAM beams is proposed and proved by simulation.

2. METHODOLOGY

The complex amplitude distribution of the Laguerre-Gaussian beam with radial index p=0 can be expressed as

$$E^l(r,\theta,z) = A \cdot exp\left[i\left(\phi - \frac{z}{z_R}\frac{r^2}{w^2} - l\theta\right)\right], \quad (1)$$

where,

SPIE-CLP Conference on Advanced Photonics 2022, edited by Xu Liu, Anatoly Zayats, Xiaocong Yuan, Proc. of SPIE Vol. 12601, 126010L
 · 0277-786X · doi: 10.1117/12.2666812

$$A = \frac{C_{pl}}{w_0} \cdot \left(\frac{\sqrt{2}r}{w}\right)^{|l|} \cdot L_p^{|l|}\left(\frac{2r^2}{w^2}\right) \cdot exp\left(-\frac{r^2}{w^2}\right),$$

r, *θ*, *z* are three parameters of cylindrical coordinates, and *l* is the azimuthal index (also called the topological charge of OAM beam). C_{pl} is a normalized constant, w_0 is the beam waist of the fundamental mode, and *w* is the radius of the OAM beam and can be expressed as $w = w_0\sqrt{1 + (z/z_R)^2}$. $z_R = \pi w_0^2/\lambda$ is the Rayleigh distance, the term $L_0^{|l|}(x)$ represents the generalized Laguerre polynomial, and $\phi = (l + 2p + 1)arctan(z/z_R)$ is the Gouy phase.

The schematic diagram of the proposed method is shown in Figure 1.

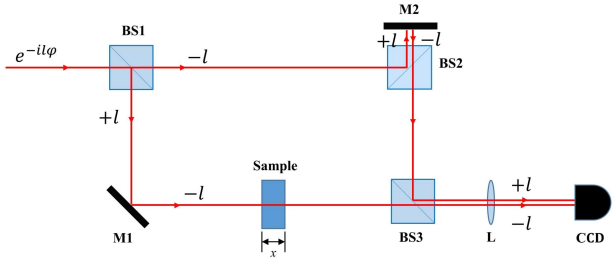

Figure 1. Schematic diagram of the proposed method. BS1-BS3, beam splitters; M1, M2, mirrors; L, lens; CCD, charge coupled device. M2 is used to introduce an additional reflection, so that the sign of the OAM of the reference beam that arrives at the CCD is opposite to that of the measurement beam.

Two OAM beams with opposite signs are used as a measurement path and a reference path, and a petal like pattern is produced in the imaging plane of the CCD. If an RI variation sample is placed in the measurement path, the phase difference between the measurement and reference paths is

$$\Delta\psi = \psi_{-l} - \psi_{+l} = \left(\phi_{-l} - \frac{z_a}{z_R}\frac{r^2}{w^2} - l\theta + \varphi(t)\right) - \left(\phi_{+l} - \frac{z_b}{z_R}\frac{r^2}{w^2} + l\theta\right) = \varphi(t) - 2l\theta + \varphi_0, \quad (2)$$

where, $\varphi(t)$ is the time variable phase delay introduced by the RI sample. And φ_0 is the constant phase difference between the measurement and reference paths, which is caused by the difference in the optical path length without regard to the RI variation of the sample. The angular position of the bright spots of the petal-like pattern can be estimated when set $\Delta\psi = 2m\pi$ $(m = 0,1,2,3\ldots)$. According to Eq. (2) and taking the derivative with respect to time, we obtain

$$\frac{d\varphi}{dt} = 2l\frac{d\theta}{dt}. \quad (3)$$

The phase difference $\Delta\varphi$ caused by the RI changes is equal to

$$\Delta\varphi = \varphi(t) - \varphi(0) = \frac{2\pi}{\lambda} \cdot [n(t) - n(0)] \cdot x, \quad (4)$$

where, *x* is the length of the sample. Taking the derivative with respect to time again yields

$$\frac{d\varphi}{dt} = \frac{2\pi}{\lambda} \cdot \frac{dn}{dt} \cdot x. \quad (5)$$

Combining Eq. (3) and Eq. (5), the RI variation rate dn/dt is proportional to the rotation angular velocity of the petal-like pattern $d\theta/dt$ by

$$\frac{dn}{dt} = \frac{\lambda l}{\pi x} \cdot \frac{d\theta}{dt}. \quad (6)$$

In previous reports, $d\theta/dt$ was estimated by measuring the rotation angle $d\theta$ of the bright spots of the petal-like pattern over a tiny time interval dt. This method results in a relatively large error, because it is difficult to determine the center of spots precisely. Especially in the actual experimental environment, the shape of the spots may be distorted due to various external disturbances. In this letter, we propose an approach of using the normalized cross correlation (NCC) method to estimate $d\theta/dt$[12]. The value range of the correlation coefficient γ of two images is [-1, 1], the larger the value of γ is, the higher the similarity between two images. When the petal-like spots rotate by an angle of $2\pi/2l$, the

correlation coefficient γ of two interference images changes by one cycle. Hence, $d\theta/dt$ can be estimated by calculating the frequency f of the time evolution of the correlation coefficient γ according to

$$f = \frac{1}{\frac{2\pi}{2l}\left/\frac{d\theta}{dt}\right.}, \tag{7}$$

where f can be obtained by taking the Fourier transform of the time evolution of the correlation coefficient if RI varies at a constant rate. However, in the case that RI varies nonuniformly, temporal information is indispensable and cannot be obtained when taking the Fourier transform, hence a time-frequency analysis is needed for analyzing the time evolution of the correlation coefficient. In this letter, the short-time Fourier transform (STFT) method is adopted to link the time domain and frequency domain of the time varying correlation coefficient together[13].

3. SIMULATION RESULTS

The petal-like pattern produced by interference is shown in Figure 2. Here the topological charges of OAM beams are set to l = ±2. Taking the Figure 2(a) for a reference, the correlation coefficient γ changes by a period when the phase difference $\Delta\varphi$ changes from 0 to 2π.

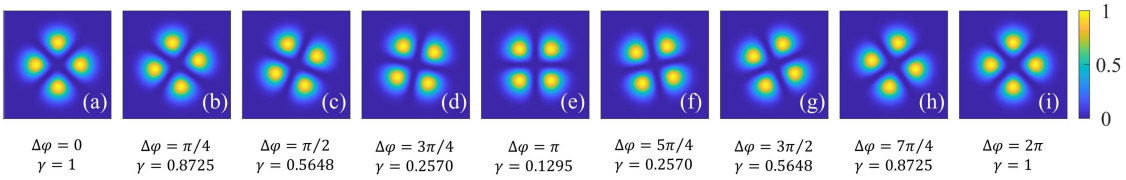

Figure 2. The petal-like pattern produced by the interference of OAM beams with l = ±2 when $\Delta\varphi$ is at different values. The spots rotate when the phase difference of two OAM beams changes, the correlation coefficient γ changes with the phase difference, and one cycle of the correlation coefficient corresponds to a phase difference change of 2π.

To demonstrate the feasibility of the proposed method, three different RI models and estimation of their variation rate are simulated in this section. Figure 3(a) shows model 1, the RI increases with time in 200 s at a constant variation rate of 1.773×10^{-5} s^{-1}. The simulated length of the sample is set to 3 cm. The phase difference caused by RI variation is calculated according to Eq. (4). The time variation of its corresponding correlation coefficient is shown in Figure 3(b), it can be seen that the frequency remains the same and can be estimated by taking the Fourier transform. Figure 3(c) shows the Fourier transform result of the correlation coefficient time evolution. The frequency of the intensity peak $f \approx 1$ Hz. According to Eq. (6) and Eq. (7), the calculated RI variation rate is 1.773×10^{-5} s^{-1}, which is consistent with the theoretical value.

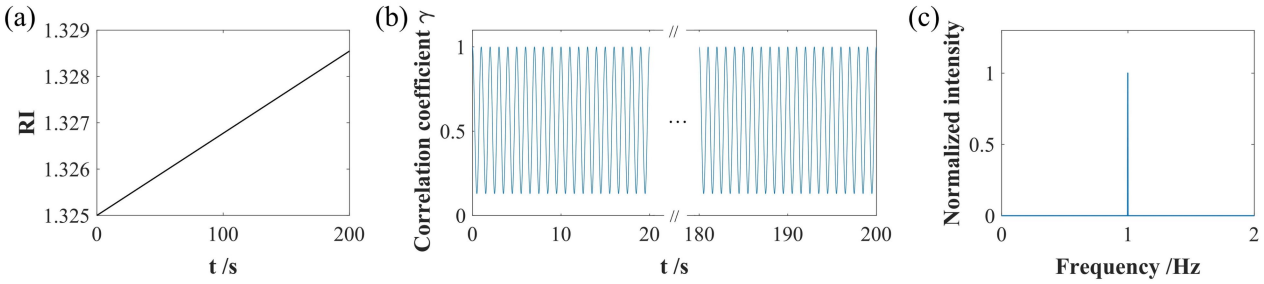

Figure 3. (a) RI model 1, RI increases with time in 200s at a constant variation rate of 1.773×10^{-5} s^{-1}. (b) Time evolution of the correlation coefficient of model 1. (c) The Fourier transform result of the correlation coefficient time evolution of model 1. The frequency of the intensity peak is 1 Hz.

A polygonal line RI model is simulated in model 2, which is shown in Figure 4(a). The RI increases with a variation rate of 4.433×10^{-5} s^{-1} from 0 s to 40 s, 1.773×10^{-5} s^{-1} from 40 s to 140 s and 2.956×10^{-5} s^{-1} from 140 s to 200 s. Figure 4(b) shows the corresponding time evolution of correlation coefficient. The change in the RI variation rate gives rise to the change in the frequency of γ. Figure 4(c) shows the Fourier transform result of the correlation coefficient shown in Figure 5(b), the corresponding frequencies of the three intensity peaks are 1 Hz, 1.667 Hz and 2.5 Hz. The RI variation rate is calculated to be 1.773×10^{-5} s^{-1}, 2.956×10^{-5} s^{-1} and 4.433×10^{-5} s^{-1}. The results are equal to the theoretical values, but the important temporal information is lost. To extract information about time, a time-frequency analysis method is indispensable, here the STFT method is adopted. Figure 4(d) shows the 3D diagram of the result of the correlation coefficient by use of STFT method, the horizontal axis represents time, the vertical axis represents frequency, and the color bar is the normalized intensity. The temporal information and frequency information can be read from Figure 4(d) simultaneously. The RI variation rate of model 2 calculated according to Eq. (6) and Eq. (7) is shown in Figure 4(e). The calculated results are in good agreement with the theoretical values.

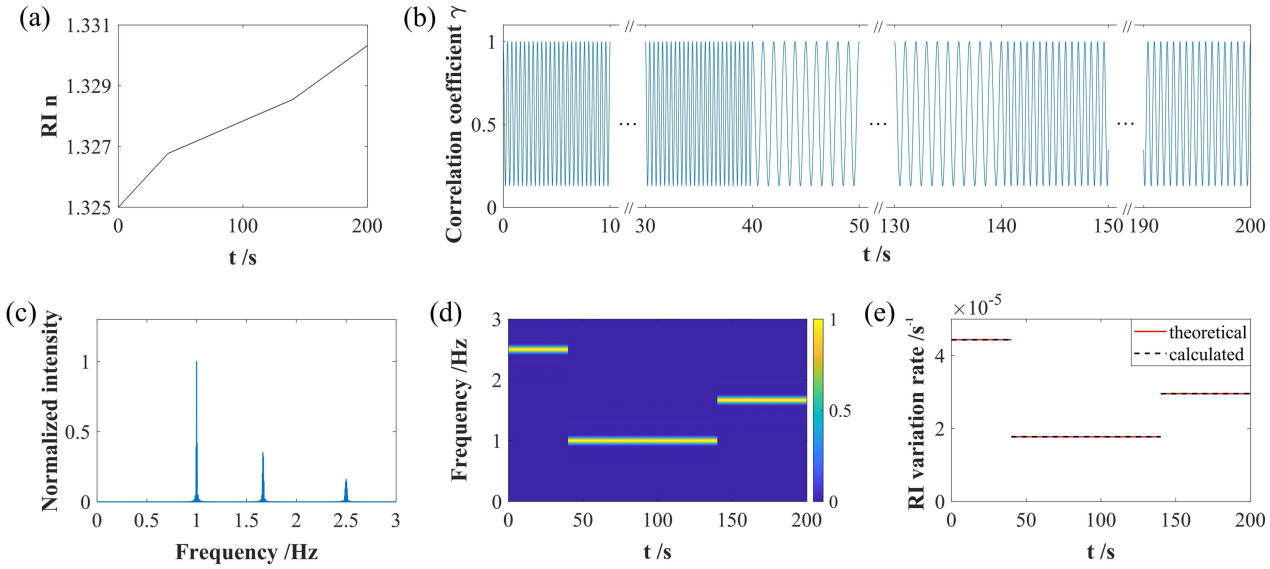

Figure 4. The simulated results of model 2. (a) The time variation of RI. The RI variation rates are 4.433×10^{-5} s^{-1}, 1.773×10^{-5} s^{-1} and 2.956×10^{-5} s^{-1} from 0 s to 40 s, 40 s to 140 s and 140 s to 200 s, respectively. (b) Time evolution of the correlation coefficient of model 2. (c) The Fourier transform result of the correlation coefficient time evolution of model 2. The frequencies of the three intensity peaks are 1 Hz, 1.667 Hz and 2.5 Hz. (d) The time-frequency analysis result of the correlation coefficient time evolution of model 2 by use of the STFT method, the color bar represents normalized intensity. (e) The RI variation rate calculated by using the proposed method (black dotted line) and the theoretical RI variation rate (red solid line) of model 2.

To further prove the necessity of the time-frequency analysis method, model 3 of an increasing RI but of a decreasing RI variation rate is simulated. The simulation results are shown in Figure 5. As seen in Figure 5(b), the frequency of the correlation coefficient of model 3 decreases gradually and is different at every moment. Figure 5(c) shows the Fourier transform result of the time evolution of the correlation coefficient. The frequency information at different moments is mixed together and difficult to distinguish, and the temporal information is not revealed. Figure 5 (d) is the time frequency analysis result of the correlation coefficient, and temporal information is included in it. Figure 5(e) shows the calculated result of the RI variation rate and the theoretical value, which overlap very well.

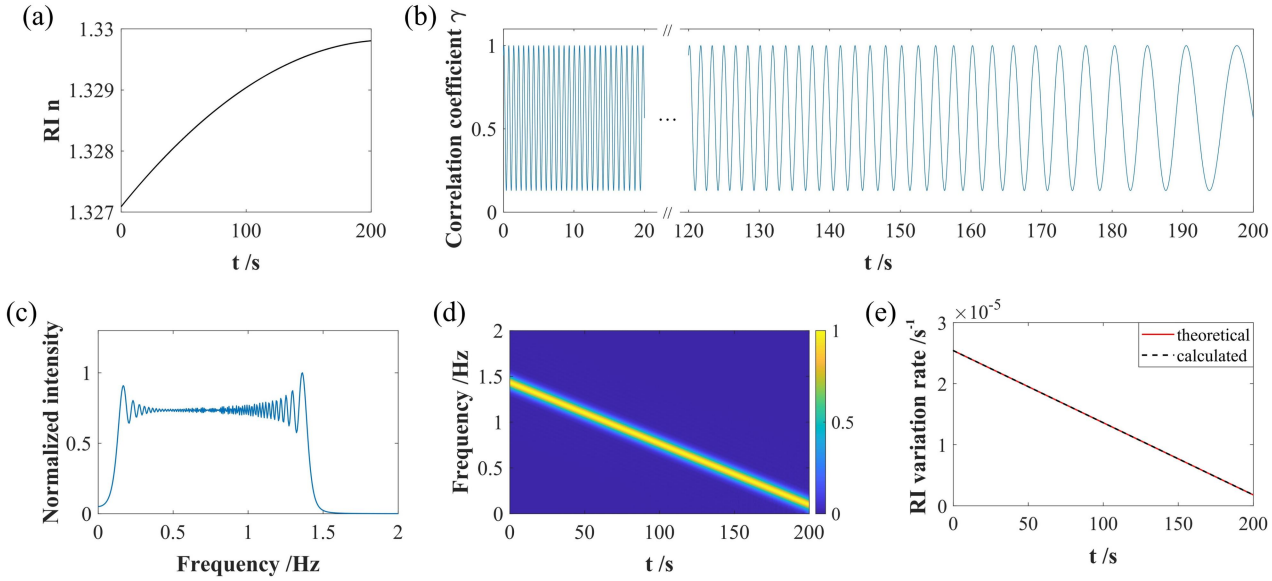

Figure 5. The simulated result of model 3. (a) The time variation of RI, the RI increases but the variation rate decreases gradually. (b) Time evolution of the correlation coefficient of model 3. (c) The Fourier transform result of the correlation coefficient time evolution of model 3. (d) The time-frequency analysis result of the correlation coefficient time evolution of model 3 by use of the STFT method, the color bar represents normalized intensity. (e) The RI variation rate calculated by using the proposed method (black dotted line) and the theoretical RI variation rate (red solid line) of model 3.

4. CONCLUSIONS

In summary, a detection method of the small variation rate of RI based on OAM interferometry and time-frequency analysis is proposed in this letter, which is simple in structure. Uniform and nonuniform RI models are simulated, their RI variation rates are calculated using the proposed method, and the results are in line with expectations. The NCC method is used to avoid the error of determining the center of spots when measuring the rotation angle of petal-like spots. The introduction of the time-frequency analysis method makes possible to detect the variation rate of RI at every moment when RI varies at a nonuniform rate. This method also extends a new approach to measure tiny velocity or other physical coefficients of RI such as the spatial gradient of RI of gradient index flat glass or the temperature coefficient of RI.

REFERENCES

[1] Belmonte, A., Rosales-Guzmán, C. and Torres, J. P., "Measurement of flow vorticity with helical beams of light," Optica 2(11), 1002-1005 (2015).
[2] Jantzi, A., Jemison, W., Laux, A., Mullen, L. and Cochenour, B., "Enhanced underwater ranging using an optical vortex, " Opt. Express 26(3), 2668-2674 (2018).
[3] Cvijetic, N., Milione, G., Ip, E. and Wang, T., "Detecting lateral motion using light's orbital angular momentum, " Sci. Rep. 5(1), 1-7 (2015).
[4] Guo, J., Ming, S., Wu, Y., Chen, L. Q. and Zhang, W., "Super-sensitive rotation measurement with an orbital angular momentum atom-light hybrid interferometer," Opt. Express 29(1), 208-218 (2021).
[5] Qiu, L. Q., Hu, H. F., Zhao, Y., Li, J. and Wang, Q., "Fiber optic temperature sensor using the orbital angular momentum and gaussian beams," INSTRUM SCI TECHNOL 45(2), 123-136 (2017).

[6] Greenberg, A. P., Prabhakar, G. and Ramachandran, S., "High resolution spectral metrology leveraging topologically enhanced optical activity in fibers, " Nat. Commun. 11(1), 1-7 (2020).
[7] Yu, S., Pang, F., Liu, H., Li, X., Yang, J. and Wang, T., "Compositing orbital angular momentum beams in Bi4Ge3O12 crystal for magnetic field sensing, " Appl. Phys. Lett. 111(9), 091107 (2017).
[8] Zhu, J., Wang, L., Ji, J. and Zhao, S., "Real-time measurement of dynamic micro-displacement and direction using light's orbital angular momentum, " Appl. Phys. Lett. 120(25), 251104 (2022).
[9] Zhang, Z., Cen, L., Wang, F. and Zhao, Y., "Tiny velocity measurement using rotating petal-like mode of orbital angular momentum, " Opt. Lett. 46(19), 4805-4808 (2021).
[10] Zhai, Y., Fu, S., Yin, C., Zhou, H. and Gao, C., "Detection of angular acceleration based on optical rotational Doppler effect, " Opt. Express 27(11), 15518-15527 (2019).
[11] Dorrah, A. H., Zamboni-Rached, M. and Mojahedi, M., "Experimental demonstration of tunable refractometer based on orbital angular momentum of longitudinally structured light," Light Sci. Appl. 7(1), 1-12(2018).
[12] Zhao, D., Li, N., Ma, Y. and Chu, W., "Characteristics of Double-Vortex Optical Interferogram Based on Shearing Interference," Laser Optoelectron. Prog. 58(11), 1108001 (2021)
[13] Welch, P., "The use of fast Fourier transform for the estimation of power spectra: A method based on time averaging over short, modified periodograms, " IEEE Trans. Audio Electroacoust. 15(2), 70–73 (1967).